Frontiers in Bioscience Elite

Front. Biosci. (Elite Ed) **2026**; 18(1): 44274
https://doi.org/10.31083/FBE44274

Original Research

AAV9-Mediated Targeting of Defined Neuronal Populations in Spinal Cord Through Intrathecal Injection

Tatyana Ageeva[1], Rezeda Shigapova[1,*], Eldar Davletshin[1], Elizaveta Plotnikova[1], Albert Rizvanov[1,2], Yana Mukhamedshina[1,2,3]

[1]OpenLab Gene and Cell Technologies, Institute of Fundamental Medicine and Biology, Kazan Federal University, 420008 Kazan, Russia
[2]Division of Medical and Biological Sciences, Tatarstan Academy of Sciences, 420111 Kazan, Russia
[3]Department of Histology, Cytology and Embryology, Kazan State Medical University, 420012 Kazan, Russia
*Correspondence: shigapova.r.r.7@gmail.com (Rezeda Shigapova)
Academic Editor: Baohong Zhang
Submitted: 26 June 2025 Revised: 1 October 2025 Accepted: 17 October 2025 Published: 9 February 2026

Abstract

Background: Adeno-associated viruses (AAVs) are established vectors for efficient gene delivery to the central nervous system (CNS). Increasingly, strategies aim to restrict transduction to specific neuronal subtypes defined by the associated functional properties, thereby enhancing precision and therapeutic potential. **Methods**: Recombinant AAV9 vectors carrying fluorescent reporters under the control of cytomegalovirus (CMV), human synapsin (hSyn), or homeobox 9 (Hb9) promoters were delivered intrathecally in Wistar rats. Transgene expression was evaluated 7 days post-injection by confocal microscopy. Neurons in laminae VII–X were quantified across cervical, thoracic, lumbar, and sacral spinal cord levels. Statistical analysis was performed using the Kruskal–Wallis test followed by Mann–Whitney U tests with Bonferroni correction. **Results**: In lamina VII, consistent neuronal expression was mediated by hSyn across all spinal levels, with significantly higher transduction at cervical compared to thoracic and lumbar regions ($p < 0.01$). CMV and Hb9 showed no detectable tropism for this lamina. In lamina VIII, CMV drove markedly higher expression than hSyn and Hb9, with a 2.8-fold difference at the lumbar level ($p < 0.001$). In lamina X, CMV expression exceeded hSyn at the lumbar and sacral levels ($p < 0.05$), while Hb9 showed no activity. In lamina IX, all promoters mediated motoneuron transduction, but only Hb9 restricted expression specifically to motoneuron somata. Notably, CMV induced off-target expression in glial cells. **Conclusions**: AAV9-mediated expression patterns in the spinal cord are strongly shaped by promoter choice and segmental level. Hb9 provides high motoneuron specificity, hSyn supports broad neuronal activation across laminae VII–X, whereas CMV drives robust but non-specific expression with significant off-target activity. These findings highlight the importance of rational promoter selection for spinal cord gene therapy and strategies aimed at functional recovery in motor system disorders.

Keywords: adeno-associated virus; spinal cord; motor neurons; gene therapy; promoter regions; intrathecal injections

1. Introduction

Adeno-associated viruses (AAV) continue to be considered powerful tools in the field of neurobiology and gene therapy due to their ability to efficiently transfer genetic material into cells, including neurons [1,2]. According to known studies, the pattern of AAV biodistribution has significant differences due to a number of reasons, including the animal model used, the serotype of the vector, the method used to assess biodistribution, the method of administration of the gene product, determining different results and difficulties in translating the described preclinical results [3–7]. A review of the literature over the last decade on AAV-based gene therapies targeting the central nervous system (CNS) highlights the limited knowledge available on the biodistribution of AAVs within the spinal cord grey matter laminae and the need to continue these studies [7–10]. Cell-selective gene expression is a critical element of many AAV-based vector gene therapies. Given the frequent use of highly transcriptionally active promoters as part of genetic constructs that define potent gene expression in neural tissue, neuron-specific promoters are largely more successful at minimising off-target transgene expression [11,12].

Among delivery strategies, intrathecal administration has emerged as a particularly promising approach, as introduction into cerebrospinal fluid enables broad dissemination of AAV across spinal segments while minimizing parenchymal injury [13,14]. In preclinical models, this route has achieved robust gene transfer throughout the spinal cord and dorsal root ganglia [15], and has been applied for widespread therapeutic delivery in disorders such as spinal muscular atrophy and hereditary spastic paraplegia [16].

Despite this translational potential, little is known about how intrathecal delivery shapes viral biodistribution across spinal segments and within defined gray matter laminae, particularly with respect to the interaction of neuron-selective promoters with distinct neuronal populations. In particular, it is known that transgene expression under the human synapsin (hSyn) promoter was concentrated in neurons located within laminae IV–VIII and

X, with some expression in lamina IX, while the homeobox 9 (Hb9) promoter successfully restricted transgene expression almost exclusively to motor neurons in lamina IX when considering only the lumbar spinal cord [9,17]. In contrast, quantification of transduced cells in each region of the three spinal cord sections showed that cytomegalovirus (CMV) promoter-driven expression resulted in significantly higher relative numbers of green fluorescent protein (GFP)-positive cells in the cervical spinal cord, but not in the lumbar spinal cord, compared to hSyn, without assessing transduced neurons in grey matter laminae [18,19]. To further understand the transcriptional activity of the described promoters, it is important to assess the biodistribution of the transgene in grey matter laminae in all parts of the spinal cord, achieved by introducing AAVs with different promoter regions, and to determine whether specific cell types of interest to the researcher will be transduced.

In this study, we focus on comparative analyses of the biodistribution of AAV depending on the type of promoter used, such as the CMV, hSyn, and Hb9 promoters. These promoters were chosen because of their specificity to neuronal cells in different grey matter laminae of the spinal cord. Understanding how promoters affect gene expression in specific neuronal populations may provide important data for the development of targeted gene therapy and neuroimaging techniques. For example, for a number of neurodegenerative diseases, gene therapy involves transduction of specific populations of spinal cord neurons [1], such as target gene therapy for motor neurons located in laminae VIII and IX (ventral horn) of the grey matter of the spinal cord in severe spinal muscular atrophy (SMA), targeted therapy for the loss of lumbar interneurons between laminae IV and VII grey matter of the spinal cord and α-motoneurons in the ventral horn in the cervical, thoracic, and lumbar spinal cord in amyotrophic lateral sclerosis (ALS), and gene activation of lumbar central pattern generator (CPG) neurons and their remaining inputs, both sensory afferents and propriospinal networks, dispersed at all levels of the spinal cord, which may be potential targets for CPG re-activation for functional recovery from spinal cord injury [8,20,21].

The purpose of this study is to assess the biodistribution of AAV vectors in the central nervous system, with a focus on the spinal cord and neuronal transduction of different grey matter laminae. We analysed the activity of the CMV, hSyn, and Hb9 promoters on the specificity of fluorescent protein expression in neurons, allowing us to determine their efficacy and targeting for potentialtherapeutic applications.

2. Materials and Methods

2.1 Genetic Construct Design

The plasmids pAAV-Hb9-LMO3 (sbGLuc-VChR1-eYFP) and pAAV-hSyn-mCherry were synthesized by Addgene, Watertown, MA, USA (Addgene plasmid: 114103, catalog #114472) according to a previously reported specification [17]. A schematic representation of the developed constructs is shown in Fig. 1A. Luminopsin (LMO3) is a fusion protein of Gaussia luciferase variant (sbGLuc), Volvox canalorhodopsin-1 (VChR1) and enhanced yellow fluorescent protein (eYFP) under the regulation of the Homeobox 9 (Hb9) promoter. The plasmid pAAV-CMV-eGFP was provided by Marlin Biotech, Moscow, Russia.

2.2 Production of Plasmid DNA for AAVs Assembly

To produce plasmid DNA of pAAV-Hb9-LMO3 (sbGLuc-VChR1-eYFP), pAAV-hSyn-mCherry, pAAV-CMV-eGFP in preparative quantities, the Escherichia coli strain NEB® Stable (Thermo Fisher Scientific Inc., Waltham, MA, USA) was transformed. For this purpose, bacterial cells were cultured in Luria-Bertani (LS-LB) medium without addition of antibiotics at 37 °C and vigorous shaking (200–300 rpm) until OD600 = 0.30–0.35. In this work, low-salt Luria-Bertani LS-LB medium was used for cultivation of E. coli NEB® Stable cells (per 1 L of deionized water): salt-free yeast extract (Sigma-Aldrich, St. Louis, MI, USA USA)—5 g, tryptone (Sigma-Aldrich, USA)—10 g, 5 M NaCl (Sigma-Aldrich, USA)—5 g, pH 7.5. Agarized LS-LB medium was also used (per 1 L of deionized water): salt-free yeast extract—5 g, tryptone—10 g, 5 M NaCl—5 g, agar (Sigma-Aldrich, USA)—15 g. Sterilization of nutrient media was carried out in autoclave in liquid or agar mode. Competent cells were prepared using $CaCl_2$ method. Plasmid DNA from bacterial cells was isolated by alkaline lysis using a commercial GeneJET Plasmid MiniprepKit (Thermo Fisher Scientific Inc., USA) according to the methodology recommended by the manufacturer. For this purpose, a single bacterial colony of recombinant Escherichia coli NEB® Stable strain containing the required plasmid DNA was seeded in a flask with 2–5 mL of LS-LB medium in the appropriate selective antibiotic. The culture was incubated in a shaker (300 rpm) at 37 °C for 8 hours. Next, the initial bacterial culture was diluted from 1:500 in 50 mL of LB medium. After seeding, the culture was incubated in a shaker (300 rpm) at 37 °C for 12–16 hours. The culture should reach a cell density of approximately 3–4 $\times$ 10^9 cells per 1 mL. Bacterial cells were harvested by centrifugation in 50 mL tubes at 6000 g for 15 min at 4 °C. Plasmid DNA was isolated from the obtained bacterial biomass.

2.3 Transfection and Immunofluorescence Analysis

SH-SY5Y cells were cultured in DMEM/F-12 medium (PanEco, Moscow, Russia) supplemented with 10% fetal bovine serum (Bioserum, South America), 2 mM L-glutamine (PanEco, Russia) and 1$\times$ penicillin and streptomycin antibiotic mixture (PanEco, Russia). Cells were cultured in an incubator at 37 °C in a humidified atmosphere containing 5% CO_2. The transfection agent

linear polyethylenimine (LPEI) (Thermo Fisher Scientific Inc., USA) was used to transfect SH-SY5Y cells with plasmid DNA. For transfection, SH-SY5Y cells were cultured on 6-well culture plates. A cell culture with a monolayer density of 60–70% was used. To 400 µL of serum-free culture medium, 2 µL of LPEI transfection agent was added, and the mixture was thoroughly mixed on a vortex. 2 µg of plasmid DNA—pAAV-Hb9-LMO3 or pAAV-hSyn-mCherry or pAAV-eGFP were added to the mixture, the mixture was thoroughly mixed, precipitated and incubated at room temperature for 15–20 min. Then 400 µL of the transfection mixture was added dropwise to the wells of the culture plate. The plate was gently shaken to achieve uniform distribution of the complexes immediately after the addition of the transfection reagent. The plates were incubated in an incubator at 37 °C in a humidified atmosphere containing 5% CO_2. Transgene expression was analyzed after 24–48 hours. For immunofluorescence analysis, the cells were fixed in 4% buffered formalin, washed with 0.1% Triton X-100 in PBS and counterstained with 4′,6-Diamidino-2-phenylindole (DAPI) (10 mg/mL in PBS, Sigma, St. Louis, MI, USA) to visualize the nuclei. The results were analyzed using an LSM 780 Confocal Microscope (Carl Zeiss, Jena, Germany).

2.4 Cell Culture

Human embryonic kidney 293 cells (HEK293T; ATCC CRL-11268, American Type Culture Collection, Manassas, VA, USA) were used in this study. The cells were cultured in high-glucose DMEM (Gibco, Waltham, MA, USA) supplemented with 10% (v/v) fetal bovine serum (FBS; Biosera Europe, France) and Penicillin-Streptomycin (Pen-Strep). All cell lines were maintained at 37 °C in a humidified atmosphere of 5% CO_2 and 95% relative humidity, and were confirmed to be free of mycoplasma contamination by PCR testing. Cell line authentication was performed by the American Type Culture Collection using short tandem repeat (STR) profiling.

2.5 Primary Motor Neuron Isolation, Culture de novo, and AAV Transduction

Primary motor neurons were isolated from neonatal Wistar rats at postnatal day 3 (P3). Animals were euthanized by decapitation (a detailed description of the procedure is provided in Section 2.9), after which the spinal cord was extracted and transferred into sterile physiological saline supplemented with antibiotics. Tissue was then incubated in 0.25% trypsin solution (PanEco, Russia) containing antibiotics at 37 °C for 20 minutes with gentle trituration every 10 minutes. Following enzymatic digestion, the suspension was centrifuged at 2000 rpm for 10 minutes. The supernatant was discarded, and the pellet was resuspended in calcium- and magnesium-free Dulbecco's phosphate-buffered saline (DPBS, 450 mL), followed by a second centrifugation under the same conditions. The DPBS wash was repeated twice. After the final centrifugation, cells were resuspended in DMEM/F12 medium without glutamine (PanEco) supplemented with B27 (ncB27 Supplement, serum-free, Shownin, Hefei, China) and EGF (1:4464, Cloud-Clone, catalog #APA560Hu02, USA). Cells were seeded into 6-well plates pre-coated 24 hours in advance with human fibronectin (IMTEK, Moscow, Russia). An initial small volume of the cell suspension was added to allow attachment; after 10–15 minutes of incubation at 37 °C, the final volume of culture medium was added. These preparations were established as *de novo* primary motor neuron cultures. Cultures were maintained under standard conditions (37 °C, 5% CO_2, 95% relative humidity) and monitored daily. Medium replacement was performed as needed but not earlier than day 3; only 50% of the medium volume was replaced during each change. Culture was confirmed to be free of mycoplasma contamination by PCR testing. On day 7 of culture, cells were transduced with recombinant AAV9 vectors (AAV9-Hb9-LMO3 or AAV9-hSyn-mCherry) at a multiplicity of infection (MOI) of 50,000. Transgene expression was evaluated 48 hours post-transduction. For immunofluorescence analysis, cells were fixed with 4% paraformaldehyde in PBS, permeabilized with 0.1% Triton X-100 in PBS, and stained with DAPI (10 mg/mL, Sigma-Aldrich) to visualize nuclei. Confocal imaging was performed using an LSM 780 microscope (Carl Zeiss, Germany). To verify the cellular identity within the cultures, immunofluorescent staining was performed using antibodies against neurons (NeuN, catalog #DF614, Affinity, Shanghai, China)/βIII-tubulin (Tuj1, catalog #AF700, Affinity, China), and astrocytes (GFAP, catalog #PAA068Ra01, Cloud-Clone Corp.), confirming the neuronal phenotype of the majority of cells; representative images are shown in **Supplementary Fig. 1**.

2.6 Production of Recombinant AAVs for Intrathecal Injection

Recombinant viral vectors AAV9-Hb9-LMO3, AAV9-hSyn-mCherry, AAV9-eGFP were produced in HEK293T cells by the triple transient transfection method on a total area of 7500 cm^2. Viral preparations were purified from cellular debris, impurity proteins, and empty viral capsids according to the methodology previously developed in the laboratory [22–24]. Viral vector preparations were sterilised by filtration using a syringe filter with a pore diameter of 0.22 µm, then frozen in viral preparation storage buffer: 1×PBS/213 mM NaCl/0.001%, Pluronic F-68 in Eppendorf tubes. Aliquots of viral preparations were taken before freezing for quality control. The viral titer was determined through quantitative PCR using primers (forward: 5′-3′-GGAACCCCCCTAGTGATGGAGTT and reverse: 5′-3′-CGGCCTCAGTGAGCGA) and a probe targeting ITRs (5′-3′(FAM) CACTCCCTCTCTCT-GCGCGCGCTCG (BBQ)). The titer of viral particles in the

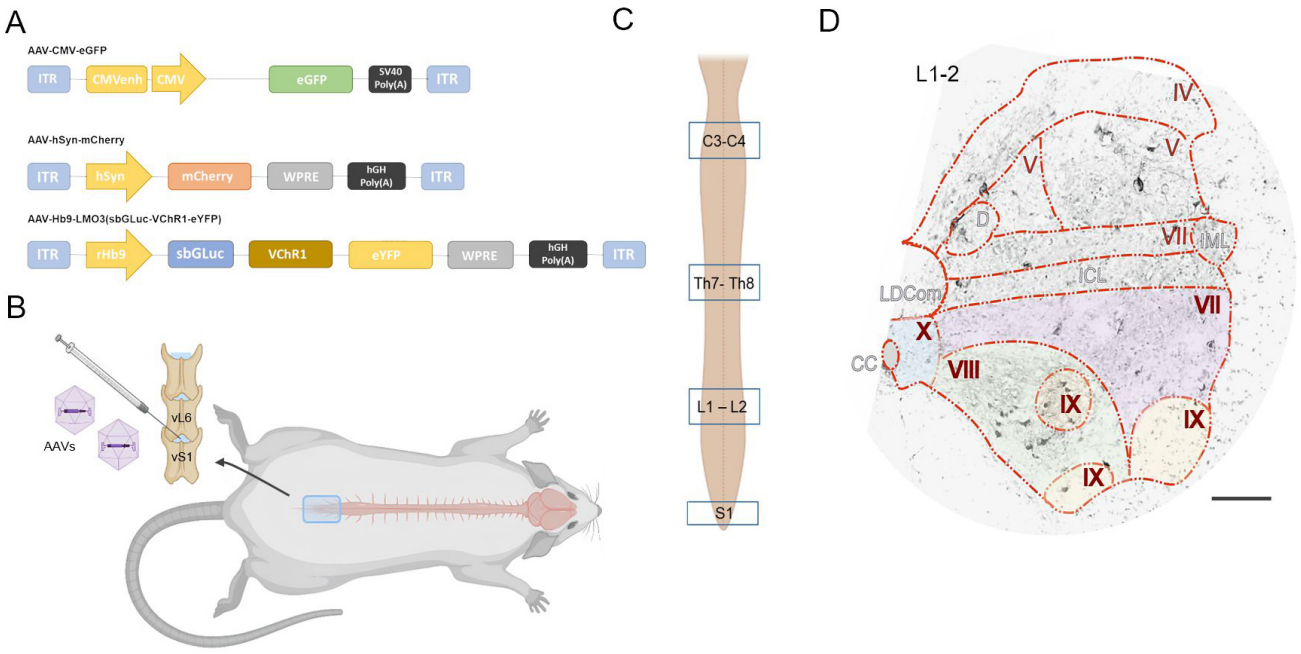

Fig. 1. Experimental design and targeting strategy for AAV-mediated gene delivery to the spinal cord. (A) Schematic representation of the main components of the gene cassette packaged into the recombinant AAV vector. (B) Intrathecal injection of gene constructs (6×10^{13} vg/mL, 20 µL) into rats: AAV9-CMV-eGFP, n = 6; AAV9-hSyn-mCherry, n = 5; AAV9-Hb9-LMO3-eYFP, n = 5. (C) Visualization of spinal cord segments used for spatial analysis of neurons expressing reporter proteins. (D) Manual mapping of reporter-positive neurons was performed using a mask that includes anatomical regions of the spinal cord, shown here at the L1–L2 segmental level. Scale bar = 100 µm. AAV, adeno-associated virus; CMV, cytomegalovirus; hSyn, human synapsin; Hb9, homeobox 9; GFP, green fluorescent protein.

final preparation was 3.52×10^{13} GC/mL for AAV9-Hb9-LMO3; 3.36×10^{13} GC/mL for AAV9-hSyn-mCherry; and 3.85×10^{13} GC/mL for AAV9-eGFP.

2.7 Animals

The study was conducted on 16 female Wistar rats (weight: 200–250 g, 3–4 months; source - KrolInfo LLC, Moscow region, Orekhovo-Zuyevsky city district, Russia). The animals were kept in standard conditions (23 °C ± 2 room temperature, 12 h:12 h light-dark cycle starting at 8 AM, 60–65% humidity, and free access to water and food ad libitum). The animals were randomly assigned into three groups: AAV9-CMV-eGFP (n = 6), AAV9-hSyn-mCherry (n = 5), AAV9-Hb9-LMO3-eYFP (n = 5). All experiments involving animals were performed in accordance with the guidelines set forth by the European Communities Council Directive 86/609/EEC. The experimental protocols were approved by the Animal Care and Use Committee of the Kazan Federal University (protocol No. 50, dated 26.09.2024).

2.8 Intrathecal Injection

Prior to the intrathecal injection procedure, the animals were anesthetized with a combination of Zoletil (Virbac Laboratories, Inc., 100 mg/mL, Karros, France) and Xylanite (Nita-Farm, Saratov, Russia). The anesthetic mixture was administered via intramuscular injection at a dose of 40 mg/kg for Zoletil and 10 mg/kg for Xylanite. All rats had the abdomen and lumbosacral area shaved at the start of the injection. The shaved areas were cleaned with a diluted solution of the alcohol-based antiseptic «Chisteya Plus» (LLC «VITA-PUL», Moscow, Russia). Rats were positioned in sternal recumbency with their pelvic limbs brought under the abdomen as cranially as possible in order to arch the lumbosacral area. The intrathecal injection was performed using a Hamilton syringe (75N 20 µL SYR 25G). The intrathecal injection of gene constructs was administered in a 20 µL, 6×10^{13} copies/mL. The injection site was between the last lumbar (L6) and the 1st sacral (S1) vertebra Fig. 1B. The injection was considered successful if one of the 2 following signs were noted: presence of CSF in the needle hub prior to injection and/or twitch of the tail during the injection. If none of these signs were noted, or if blood was visible in the needle hub prior to injection, the needle was withdrawn and another sterile needle was used to repeat the procedure. All intrathecal injections were successful at the 1st or 2nd attempt.

2.9 Euthanasia and Tissue Collection

Euthanasia was performed by intramuscular administration of Zoletil (40 mg/kg) and Xylanite (10 mg/kg), followed by transcardial perfusion with cold 0.01 M

phosphate-buffered saline (PBS; pH 7.4), followed by 4% paraformaldehyde (PFA) in PBS. For neonatal rat pups (P3), anesthesia was induced with the same drug combination at equivalent doses prior to decapitation.

For histological analysis, spinal cords were extracted and post-fixed in 4% paraformaldehyde in PBS. Tissues were cryoprotected by sequential immersion in 15% and 30% sucrose solutions. After embedding in Tissue-Tek O.C.T. Compound, 20 µm transverse sections were cut using a RWD Minux® FS800A. For each animal, five slides from each analyzed spinal cord segment (cervical C3–4, thoracic Th8–9, lumbar L1–2, and sacral S1), each containing five sections, were selected for analysis. Segment choice was based on their functional relevance: C3–4 for forelimb control, Th8–9 for trunk coordination, L1–2 for the locomotor rhythmogenic kernel, and S1 for autonomic and urinary control [25–28]. Sections were rinsed in PBS, counterstained with 4′,6-diamidino-2-phenylindole (DAPI; Sigma-Aldrich), and mounted with medium for confocal microscopy.

2.10 Sample Preparation and Confocal Microscopy

Spatial analysis of neurons expressing reporter proteins was conducted in the gray matter of the spinal cord at the level of the studied segments Fig. 1C. Detailed imaging was carried out using an LSM 780 confocal microscope (Carl Zeiss, Germany). Visualization was performed using confocal microscopy with a 20× magnification. Inverted single-channel images were used for quantitative analysis. The study was limited to the portion of the gray matter located between laminae VII and X Fig. 1D. For manual mapping of neurons, a mask encompassing the anatomical regions of the spinal cord at the L2 segment level was applied. The following structures were used as coordinate landmarks: the lateral dorsal commissural nucleus, intermediolateral nucleus, dorsal nucleus, intercalated nucleus, and the boundary between the gray and white matter.

2.11 Spatial Analysis of Neurons

Spatial analysis of neurons expressing reporter proteins was conducted in the gray matter of the spinal cord at the level of the studied segments. Visualization was performed using confocal microscopy with a 20× magnification. The study was limited to the portion of the gray matter located between laminae VII and X. For anatomical orientation, reference images from published atlases of the rat spinal cord [29] and comparative neuroanatomical studies [30]. Representative examples of these reference-based orientations, including 10× and 20× images of the central canal region. For manual mapping of neurons, a mask encompassing the anatomical regions of the spinal cord at the L2 segment level was applied. The following structures were used as landmarks: the lateral dorsal commissural nucleus (LDCom), intermediolateral nucleus (IML), dorsal nucleus (D), intercalated nucleus (ICL), and the boundary between the gray and white matter. Quantification in laminae VII, VIII, and IX was performed bilaterally, while lamina X, recognized as an asymmetrical region, was analyzed as a single area surrounding the central canal.

2.12 Statistical Software and Data Analysis Methods

Statistical analyses were performed using Origin 10.0 SR0 (OriginLab Corporation, Northampton, MA, USA). Differences among groups were first assessed using the Kruskal–Wallis test, and significant results were further examined by pairwise Mann–Whitney U tests with Bonferroni correction. Significance levels were set at $*p < 0.05$, $**p < 0.01$, and $***p < 0.001$.

3. Results

3.1 Validation of Plasmid Constructs and Transgene Expression in Vitro

To confirm the integrity and correct structure of the developed plasmid constructs, restriction digestion was performed. Analysis of pAAV-CMV-eGFP, pAAV-hSyn-mCherry, and pAAV-Hb9-LMO3-eYFP revealed restriction fragments of expected sizes, consistent with the theoretical plasmid maps (Fig. 2A). These results confirm the successful cloning and structural accuracy of the designed vectors.

To evaluate the functionality of the constructs, primary motor neuron cultures were transduced with AAV9-CMV-eGFP, AAV9-hSyn-mCherry or AAV9-Hb9-LMO3-eYFP vectors. Confocal imaging revealed expression of eGFP, mCherry or eYFP in transduced cells, confirming that both constructs drive effective transgene expression under control of the respective promoters (Fig. 2B). Notably, fluorescence was localized to neuronal pericarion, suggesting successful transduction of motor neuron populations *in vitro*.

3.2 Lamina VII

On day 7 after intrathecal administration of recombinant AAV9 vectors, the number of transduced neurons was analyzed in lamina VII at four spinal cord levels: cervical (C3–4), thoracic (Th8–9), lumbar (L1–2), and sacral (S1). No expression of reporter proteins eGFP or eYFP was detected at lamina VII in the AAV9-CMV-eGFP and AAV9-Hb9-LMO3-eYFP groups at any of the examined levels, indicating a lack of tropism of these constructs for neurons in this lamina. In contrast, the AAV9-hSyn-mCherry group exhibited consistent mCherry expression in neurons at all analyzed levels, with notable segmental variability (Fig. 3A,3A').

The highest mean number of transduced neurons was observed at C3–4 (15.88 ± 4.08). At the S1 level, the number of labeled neurons was 10.20 ± 1.70, while at Th8–9 and L1–2 the values were lower, amounting to 7.62 ± 2.74 and 6.24 ± 6.12, respectively. Despite the presence of transduced neurons at all examined levels, mCherry expression in lamina VII showed pronounced segmental hetero-

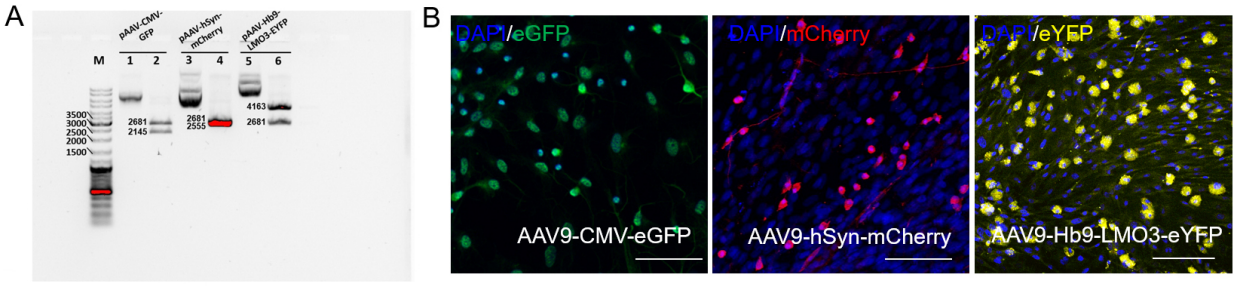

Fig. 2. Analysis of plasmid DNA integrity and transgene expression in primary motor neuron cultures. (A) Restriction analysis of plasmid DNA and electrophoresis in 0.8% agarose gel. Lanes 1, 3, 5—circular plasmid DNA; lanes 2, 4, 6—plasmid DNA after restriction digestion with SmaI. (B) Transgene expression analysis 48 hours after transduction of primary motor neuron cultures with AAV9-CMV-eGFP, AAV9-hSyn-mCherry or AAV-Hb9-LMO3-eYFP. Scale bar: 100 µm.

geneity: the average number of labeled cells was lower at the thoracic and lumbar levels compared to the cervical and sacral levels. Statistical analysis revealed a significant reduction in the number of transduced neurons at Th8–9 (p = 0.006) and L1–2 (p = 0.001) compared to C3–4. No statistically significant differences were observed between Th8–9, L1–2, and S1.

3.3 Lamina VIII

Transduction of neurons in lamina VIII was analyzed in the C3–4, Th8–9, L1–2, and S1 spinal cord segments on day 7 after intrathecal administration of recombinant AAV9 vectors (Fig. 3B,3B'). In the AAV9-Hb9-eYFP group, eYFP expression in neurons was minimal (on average, fewer than one cell per section), consistent with the motoneuron specificity of the Hb9 promoter and the absence of motoneurons in this region.

In the groups using a strong ubiquitous promoter (CMV) and a neuron-specific promoter (hSyn), a moderate number of transduced cells were observed. At the L1–2 level, the mean number of eGFP-positive neurons in the AAV9-CMV-eGFP group was 16.46 ± 4.61, which was approximately 2.8 folds higher than in the AAV9-hSyn-mCherry group (5.83 ± 2.54; p = 0.00034) and substantially exceeded the value in the AAV9-Hb9-eYFP group (0.71 ± 1.44; p = 0.00032). The difference between the AAV9-hSyn-mCherry and AAV9-Hb9-eYFP groups was also statistically significant (p = 0.005). A similar pattern was observed at the S1 level: the mean number of transduced neurons was 11.83 ± 3.62 in the AAV9-CMV-eGFP group, 3.61 ± 1.61 in the AAV9-hSyn-mCherry group, and 1.35 ± 1.57 in the AAV9-Hb9-eYFP group. Transduction efficiency with the CMV promoter was significantly higher than with hSyn (p = 0.000072) and Hb9 (p = 0.0093).

At the C3–4 level, a significant difference was found only between the AAV9-hSyn-mCherry and AAV9-Hb9-eYFP groups (p = 0.0000025), with markedly higher expression observed using the hSyn promoter. No statistically significant differences were detected between groups at the Th8–9 level.

3.4 Lamina X

Neuronal transduction in lamina X was analyzed in spinal cord segments C3–4, Th8–9, L1–2, and S1 on day 7 after intrathecal administration of recombinant AAV9 vectors (Fig. 3C,3C'). In the AAV9-CMV-eGFP group, eGFP expression in lamina X neurons was observed only at the L1–2 and S1 levels, where the mean number of transduced cells was 12.73 ± 4.92 and 10.15 ± 2.27, respectively. In the AAV9-hSyn-mCherry group, moderate transduction was detected in all examined segments, including C3–4 (4.58 ± 1.68), Th8–9 (4.92 ± 3.06), L1–2 (7.13 ± 2.83), and S1 (5.31 ± 4.35), without pronounced segmental differences. At the L1–2 and S1 levels, the number of transduced neurons in the AAV9-CMV-eGFP group was significantly higher than in the AAV9-hSyn-mCherry group (p = 0.0149 and p = 0.0144, respectively).

In the AAV9-Hb9-eYFP group, no eYFP expression was detected in lamina X neurons at any spinal level, which is consistent with the motoneuron-specific activity of the Hb9 promoter and the absence of such cells in this region.

3.5 Lamina IX

Transduction of neurons in lamina IX was evaluated at the spinal cord levels C3–4, Th8–9, L1–2, and S1 on day 7 after intrathecal injection of recombinant AAV9 vectors (Fig. 4A,4A'). All three groups demonstrated consistent reporter expression in accordance with the expected localization of motoneurons in this lamina. The average number of transduced neurons ranged from 3.58 ± 1.44 to 5.92 ± 1.79, with no statistically significant differences between groups at most segmental levels, except for the lumbar region.

At the L1–2 level, eGFP expression in the AAV9-CMV-eGFP group (5.92 ± 1.79) appeared higher than in the AAV9-hSyn-mCherry (4.92 ± 1.53) and AAV9-Hb9-eYFP (4.50 ± 2.03) groups; however, no statistically significant differences were found between the groups (Fig. 4B,C). Notably, eGFP expression was detected not only in neurons but also in glial cells, particularly in segments close to the intrathecal injection site (Fig. 4D).

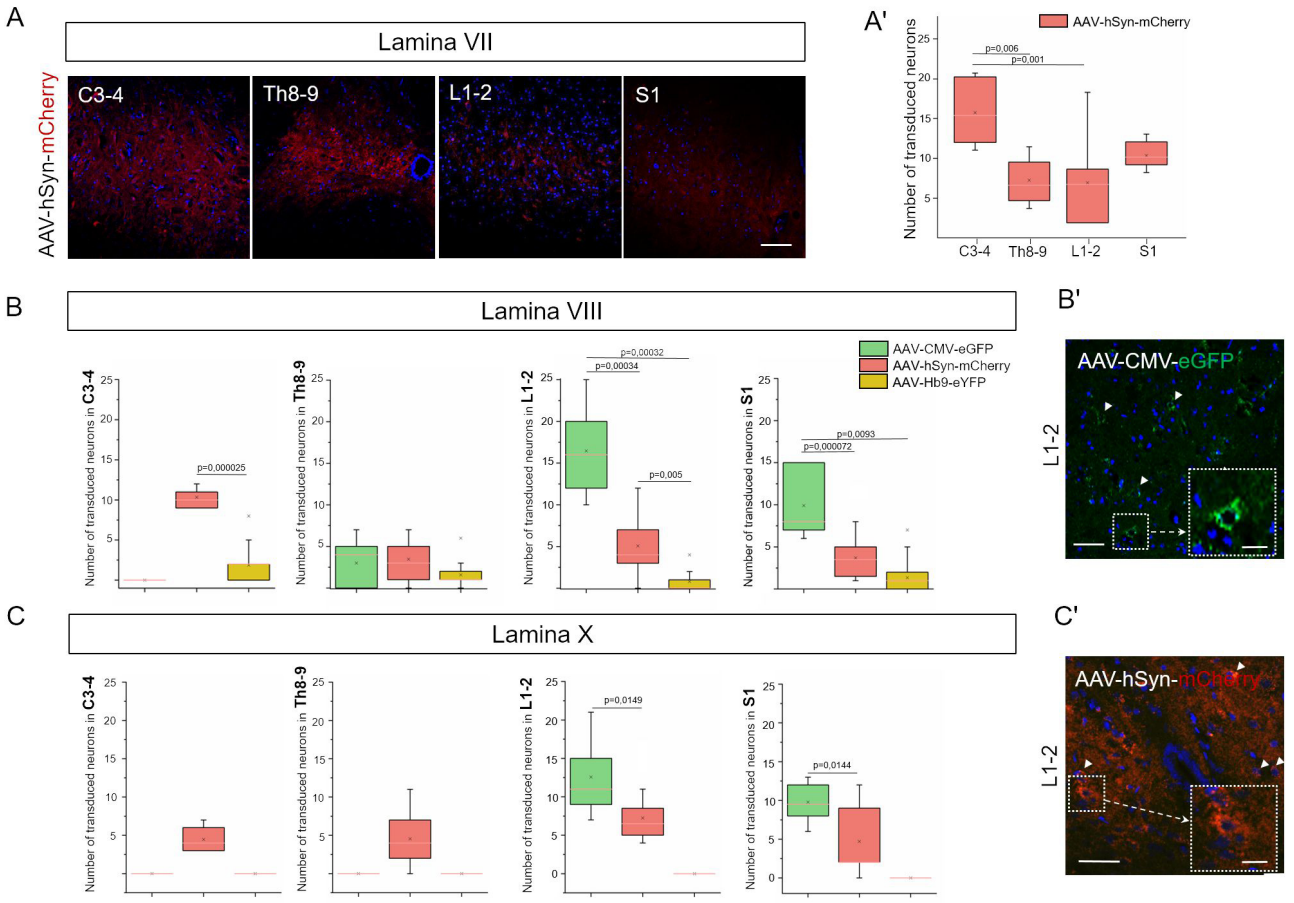

Fig. 3. Selective transduction patterns of AAV vectors in distinct spinal cord lamina. (A) Confocal images of spinal cord sections at the L1–L2 level for experimental groups. Scale bar: 60 µm. (A') Transduction of neurons in lamina VII was observed following intrathecal injection of AAV-hSyn-mCherry, whereas AAV-CMV-eGFP and AAV-Hb9-LMO3-eYFP showed no tropism for these neurons. (B) Number of transduced neurons in lamina VIII (C) and X at C3–4, Th8–9, L1–L2, and S1 spinal cord levels. Statistical analysis was performed using the Mann–Whitney U test with Bonferroni correction. (B') Confocal imaging of spinal cord lamina VIII (C') and X at the L1–L2 level in experimental groups. White arrowheads indicate transduced neurons. Insets with dashed borders show enlarged views of selected regions. Scale bar: 60 µm; inset scale bar: 15 µm.

The pattern of eYFP expression under the control of the Hb9 promoter displayed distinct characteristics compared to the other vectors: the fluorescent signal was predominantly confined to motoneuron somata, with minimal labeling of neuronal processes, in contrast to the more diffuse labeling observed in the groups with CMV and hSyn promoters.

4. Discussion

Intrathecal administration of AAV9 has proven to be a promising minimally invasive method for delivering genetic constructs to the spinal cord. This approach ensures broad vector distribution in the cerebrospinal fluid, minimizing tissue damage and increasing accessibility to lumbar enlargement neurons—a key region for restoring motor function after injury [31,32]. Unlike systemic administration, which requires overcoming the blood–brain barrier [33], intrathecal injection directly targets spinal cord networks, making it particularly important in chronic injuries when the reorganization of descending pathways (cortico–reticulo–spinal) is critical for recovery [1]. Our results are consistent with studies demonstrating that AAV9 ensures long-term expression in lumbar motoneurons [32,34,35], confirming its clinical relevance. The unique ability of AAV9 to efficiently transduce the spinal cord distinguishes it from less permeable serotypes such as AAV2 or AAV5 [34]. Our results indicate that intrathecal delivery provides an efficient means of distributing AAV9 in all segments of the spinal cord.

We observed markedly reduced transduction in cervical segments C3–4 especially under CMV and Hb9 promoters. This finding is consistent with comparative neuroanatomy, as lumbar segments contain a higher density and greater molecular diversity of motor-related interneurons such as V1 interneurons, while thoracic and cervical levels include fewer of these rhythmogenic populations

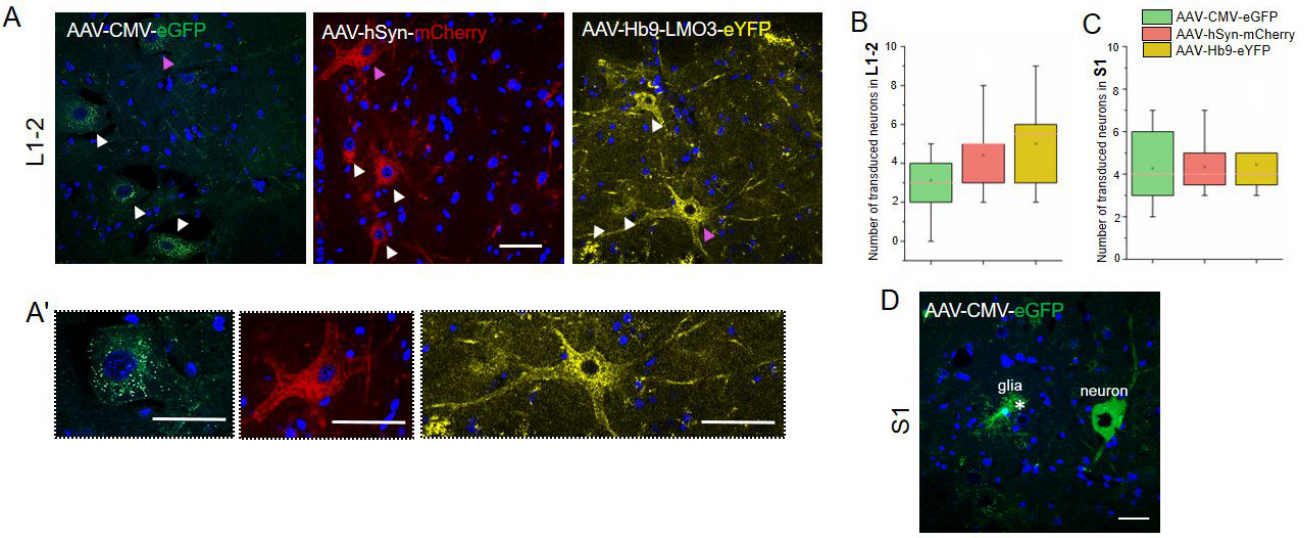

Fig. 4. Analysis of transduction specificity and distribution of AAV vectors in lamina IX of spinal cord. (A) Confocal images of spinal cord sections at the L1–L2 level showing lamina IX in experimental groups. (A') Transduced neurons are indicated by arrowheads. Higher-magnification images show motoneurons, highlighting differences in pericarion and process transduction among constructs with different promoters. (B) Number of transduced neurons in lamina IX of the L1–L2 and (C) S1 spinal cord segments on day 7 after intrathecal injection of AAV constructs. Statistical analysis was performed using the Mann–Whitney U test with Bonferroni correction. (D) In the AAV-CMV-eGFP group, reporter expression was observed in both glial cells (asterisk) and neurons within lamina IX of the S1 segment. (A,A',D) Scale bars: 50 µm. In Fig. 4A, the pink arrows indicate the neurons, which are represented on an enlarged scale in Fig. 4A'.

[36]. The thoracic segments Th8–9 are characterized by a lower density of motor-related interneurons than lumbar enlargement, which likely reduces the number of available cellular targets for promoter-driven expression and is consistent with the modest transduction observed in these regions [37]. In addition, intrathecal AAV9 delivery into caudal spinal segments produces a rostrocaudal gradient, with vector distribution diminishing rostrally and leading to lower titers in upper cervical regions [13].

The laminar patterns we observed in VII–X align with the reported positioning of locomotor CPG candidates: ventromedial interneurons in L2 (including commissural and V-class subsets) that project caudally toward L4–L5 motoneuron pools, and Hb9-positive excitatory neurons contributing to the rhythmogenic kernel [27]. This organization provides a plausible substrate for the promoter-dependent distributions detected here. In the sacral segment S1, transduction levels of all three vectors were comparable to those at lumbar L1–2. This corresponds with the functional importance of the sacral cord, where rhythmogenic circuits include the sacral micturition center localized to S1–S4 and concentrated at S1 [28,38].

The extent and selectivity of transduction is shaped by promoter choice, with our interlaminar analysis across laminae VII–X revealing distinct patterns aligned with the functional organization of spinal circuits. In combination with the Hb9 promoter, which selectively drives expression in motoneurons of lamina IX [34], our AAV9-Hb9-LMO3-eYFP construct showed high specificity. By contrast, the hSyn promoter induced broader neuronal expression across laminae VII–X, while CMV, although highly active, lacked selectivity and also transduced glial cells [39]. Although different fluorescent reporters (eGFP, mCherry, eYFP) were used, their properties do not influence cellular tropism; all vectors shared the same AAV9 backbone, production protocol, and delivery route. The distinct laminar patterns therefore reflect promoter specificity, consistent with previous studies reporting broad CMV activity [39], pan-neuronal hSyn expression, and Hb9 restriction to motoneurons [34].

For example, in lamina VIII, CMV led to overexpression in V3 neurons, which regulate locomotor symmetry [35], potentially distorting motor patterns. Our data revealed pronounced differences in transduction across spinal cord laminae, highlighting their functional specialization. In lamina VII, expression was observed only with hSyn, which is associated with the presence of V2a and V2b interneurons. V2a neurons, being excitatory, participate in rhythm generation and left–right coordination [40], whereas V2b interneurons regulate the balance of flexors and extensors [41]. In lamina VIII, CMV promoter dominance is associated with the high density of V3 neurons, which ensure symmetric motor output [35]. In lamina IX, Hb9 specificity for motoneurons confirms their central role in motor signal generation, and the selective activation of these cells via LMO3 avoids interference with inhibitory

circuits (e.g., V2b), which is critical for preventing spasticity [34]. In lamina X, CMV expression in the lumbar region, particularly in V0 subpopulations, correlates with their role in coordinating forelimb and hindlimb movements [42]. At the same time, the absence of transduction in thoracic segments emphasizes the segmental differences in the organization of motor networks.

The use of luminopsin LMO3 in combination with CTZ allows for non-invasive activation of motoneurons, avoiding risks associated with optical fiber implantation [43]. The bioluminescence peak at approximately 35 minutes corresponds to CTZ pharmacokinetics [44,45], limiting the duration of stimulation but making it compatible with short rehabilitation sessions. Importantly, combining optogenetics with motor training promotes activity-dependent synaptic plasticity [17]. For instance, activation of V2a interneurons associated with respiratory and locomotor networks may synergize with our approach, further enhancing functional recovery [40]. Despite these advances, a key limitation remains the dependence on exogenous CTZ. Potential solutions include nanocarriers for intranasal delivery [46] or self-activating luminopsins [47–49]. Moreover, the long-term safety of AAV9 requires further investigation, especially in the context of immunogenicity [50,51]. Nevertheless, our strategy, combining Hb9 selectivity and the non-invasiveness of bioluminescence, paves the way for personalized therapy targeting spinal cord intrinsic networks in both injury and neurodegenerative diseases [17,52].

Our study confirms that intrathecal administration of AAV9-Hb9-LMO3-eYFP is a highly specific method for modulating motoneurons critical for movement restoration. Differences in laminar transduction reflect their functional specialization, while the combination with bioluminescent stimulation and rehabilitation establishes a foundation for novel therapeutic strategies.

5. Conclusions

This study demonstrates that the specificity of AAV9-mediated transgene expression within the spinal cord is critically determined by the choice of promoter and the targeted grey matter lamina. The Hb9 promoter reliably confined expression to motoneurons within lamina IX across lumbar, thoracic, and cervical segments, providing a highly targeted approach compared with the broader neuronal transduction achieved by hSyn or the nonspecific expression driven by CMV. These findings highlight the importance of matching promoter elements to cellular populations and laminar architecture when designing gene therapy strategies for motor system disorders.

Abbreviations

AAV, adeno-associated virus; SCI, spinal cord injury; CMV, cytomegalovirus; hSyn, human synapsin; Hb9, homeobox 9; GFP, green fluorescent protein; SMA, spinal muscular atrophy; ALS, amyotrophic lateral sclerosis; CPG, central pattern generator; LMO3, luminopsin; sbGLuc, gaussia luciferase variant; VChR1, Volvox canalorhodopsin-1; eYFP, yellow fluorescent protein; DNA, deoxyribonucleic acid; LS-LB, Luria Bertani Broth; DAPI, 4’,6-Diamidino-2-phenylindole; LPEI, linear polyethylenimine; DMEM/F-12, Dulbecco’s modified eagle medium/nutrient mixture F-12; PBS, phosphate buffered saline; DPBS, Dulbecco’s phosphate-buffered saline; MOI, multiplicity of infection; PCR, polymerase chain reaction; ITR, inverted terminal repeats; LDCom, the lateral dorsal commissural nucleus; IML, intermediolateral nucleus; D, dorsal nucleus; ICL, intercalated nucleus; CTZ, coelenterazine.

Availability of Data and Materials

The data presented in this study are available on request from the corresponding author. The data are not publicly available due to the evolving nature of the project.

Author Contributions

TA and YM designed the research study. TA, YM, AR curated the data. TA, ED, EP, and YM performed the formal analysis. AR and YM obtained funding. ED, EP, RS, and YM conducted the investigation. TA and YM developed the methodology. TA and YM managed the project. AR and YM provided resources. AR and YM supervised the work. TA wrote the original draft. YM reviewed and edited the manuscript. All authors contributed to editorial changes in the manuscript. All authors read and approved the final manuscript. All authors have participated sufficiently in the work and agreed to be accountable for all aspects of the work.

Ethics Approval and Consent to Participate

All experiments involving animals were performed in accordance with the guidelines set forth by the European Communities Council Directive 86/609/EEC. The experimental protocols were approved by the Animal Care and Use Committee of the Kazan Federal University (protocol No. 50, dated 26.09.2024).

Acknowledgment

Not applicable.

Funding

This work was supported by a grant from the Russian Science Foundation, No. 23-75-10041; https://rscf.ru/en/project/23-75-10041/ (to Y.M.)

Conflict of Interest

The authors declare no conflict of interest.

Declaration of AI and AI-Assisted Technologies in the Writing Process

During the preparation of this work the authors used ChatGPT-4o in order to check spell and grammar. After using this tool, the authors reviewed and edited the content as needed and takes full responsibility for the content of the publication.

Supplementary Material

Supplementary material associated with this article can be found, in the online version, at https://doi.org/10.31083/FBE44274.

References

[1] Hardcastle N, Boulis NM, Federici T. AAV gene delivery to the spinal cord: serotypes, methods, candidate diseases, and clinical trials. Expert Opinion on Biological Therapy. 2018; 18: 293–307. https://doi.org/10.1080/14712598.2018.1416089.

[2] Chauhan M, Daugherty AL, Khadir FE, Duzenli OF, Hoffman A, Tinklenberg JA, *et al*. AAV-DJ is superior to AAV9 for targeting brain and spinal cord, and de-targeting liver across multiple delivery routes in mice. Journal of Translational Medicine. 2024; 22: 824. https://doi.org/10.1186/s12967-024-05599-5.

[3] Vulchanova L, Schuster DJ, Belur LR, Riedl MS, Podetz-Pedersen KM, Kitto KF, *et al*. Differential adeno-associated virus mediated gene transfer to sensory neurons following intrathecal delivery by direct lumbar puncture. Molecular Pain. 2010; 6: 1744–8069. https://doi.org/10.1186/1744-8069-6-31.

[4] Liguore WA, Domire JS, Button D, Wang Y, Dufour BD, Srinivasan S, *et al*. AAV-PHP.B Administration Results in a Differential Pattern of CNS Biodistribution in Non-human Primates Compared with Mice. Molecular Therapy. 2019; 27: 2018–2037. https://doi.org/10.1016/j.ymthe.2019.07.017.

[5] Chen X, Lim DA, Lawlor MW, Dimmock D, Vite CH, Lester T, *et al*. Biodistribution of Adeno-Associated Virus Gene Therapy Following Cerebrospinal Fluid-Directed Administration. Human Gene Therapy. 2023; 34: 94–111. https://doi.org/10.1089/hum.2022.163.

[6] Rosenberg JB, Fung EK, Dyke JP, De BP, Lou H, Kelly JM, *et al*. Positron Emission Tomography Quantitative Assessment of Off-Target Whole-Body Biodistribution of I-124-Labeled Adeno-Associated Virus Capsids Administered to Cerebral Spinal Fluid. Human Gene Therapy. 2023; 34: 1095–1106. https://doi.org/10.1089/hum.2023.060.

[7] Kussick E, Johansen N, Taskin N, Chowdhury A, Quinlan MA, Fraser A, *et al*. Enhancer AAVs for targeting spinal motor neurons and descending motor pathways in rodents and macaque. Cell Reports. 2025; 44: 115730. https://doi.org/10.1016/j.celrep.2025.115730.

[8] Passini MA, Bu J, Richards AM, Treleaven CM, Sullivan JA, O'Riordan CR, *et al*. Translational fidelity of intrathecal delivery of self-complementary AAV9-survival motor neuron 1 for spinal muscular atrophy. Human Gene Therapy. 2014; 25: 619–630. https://doi.org/10.1089/hum.2014.011.

[9] Jan A, Richner M, Vægter CB, Nyengaard JR, Jensen PH. Gene Transfer in Rodent Nervous Tissue Following Hindlimb Intramuscular Delivery of Recombinant Adeno-Associated Virus Serotypes AAV2/6, AAV2/8, and AAV2/9. Neuroscience Insights. 2019; 14: 1179069519889022. https://doi.org/10.1177/1179069519889022.

[10] Beharry A, Gong Y, Kim JC, Hanlon KS, Nammour J, Hieber K, *et al*. The AAV9 Variant Capsid AAV-F Mediates Widespread Transgene Expression in Nonhuman Primate Spinal Cord After Intrathecal Administration. Human Gene Therapy. 2022; 33: 61–75. https://doi.org/10.1089/hum.2021.069.

[11] Powell SK, Samulski RJ, McCown TJ. AAV Capsid-Promoter Interactions Determine CNS Cell-Selective Gene Expression In Vivo. Molecular Therapy. 2020; 28: 1373–1380. https://doi.org/10.1016/j.ymthe.2020.03.007.

[12] Nieuwenhuis B, Haenzi B, Hilton S, Carnicer-Lombarte A, Hobo B, Verhaagen J, *et al*. Optimization of adeno-associated viral vector-mediated transduction of the corticospinal tract: comparison of four promoters. Gene Therapy. 2021; 28: 56–74. https://doi.org/10.1038/s41434-020-0169-1.

[13] Bailey RM, Rozenberg A, Gray SJ. Comparison of high-dose intracisterna magna and lumbar puncture intrathecal delivery of AAV9 in mice to treat neuropathies. Brain Research. 2020; 1739: 146832. https://doi.org/10.1016/j.brainres.2020.146832.

[14] Garza IT, Eller MM, Holmes SK, Schackmuth MK, Bailey RM. Expression and distribution of rAAV9 intrathecally administered in juvenile to adolescent mice. Gene Therapy. 2025; 32: 189–196. https://doi.org/10.1038/s41434-024-00498-2.

[15] Gong Y, Berenson A, Laheji F, Gao G, Wang D, Ng C, *et al*. Intrathecal adeno-associated viral vector-mediated gene delivery for adrenomyeloneuropathy. Human Gene Therapy. 2019; 30: 544–555. https://doi.org/10.1089/hum.2018.079.

[16] Ma W, Wu Z, Zhao T, Xia Y, Qin J, Tian X, *et al*. Preclinical evaluation of AAV9-coSMN1 gene therapy for spinal muscular atrophy: efficacy and safety in mouse models and non-human primates. Molecular Medicine. 2025; 31: 158. https://doi.org/10.1186/s10020-025-01207-4.

[17] Petersen ED, Sharkey ED, Pal A, Shafau LO, Zenchak-Petersen J, Peña AJ, *et al*. Restoring Function After Severe Spinal Cord Injury Through BioLuminescent-OptoGenetics. Frontiers in Neurology. 2022; 12: 792643. https://doi.org/10.3389/fneur.2021.792643.

[18] McLean JR, Smith GA, Rocha EM, Hayes MA, Beagan JA, Hallett PJ, *et al*. Widespread neuron-specific transgene expression in brain and spinal cord following synapsin promoter-driven AAV9 neonatal intracerebroventricular injection. Neuroscience Letters. 2014; 576: 73–78. https://doi.org/10.1016/j.neulet.2014.05.044.

[19] Lukashchuk V, Lewis KE, Coldicott I, Grierson AJ, Azzouz M. AAV9-mediated central nervous system-targeted gene delivery via cisterna magna route in mice. Molecular Therapy. Methods & Clinical Development. 2016; 3: 15055. https://doi.org/10.1038/mtm.2015.55.

[20] Bravo-Hernandez M, Tadokoro T, Navarro MR, Platoshyn O, Kobayashi Y, Marsala S, *et al*. Spinal subpial delivery of AAV9 enables widespread gene silencing and blocks motoneuron degeneration in ALS. Nature Medicine. 2020; 26: 118–130. https://doi.org/10.1038/s41591-019-0674-1.

[21] Brommer B, He M, Zhang Z, Yang Z, Page JC, Su J, *et al*. Improving hindlimb locomotor function by Non-invasive AAV-mediated manipulations of propriospinal neurons in mice with complete spinal cord injury. Nature Communications. 2021; 12: 781. https://doi.org/10.1038/s41467-021-20980-4.

[22] Zolotukhin S, Byrne BJ, Mason E, Zolotukhin I, Potter M, Chesnut K, *et al*. Recombinant adeno-associated virus purification using novel methods improves infectious titer and yield. Gene Therapy. 1999; 6: 973–985. https://doi.org/10.1038/sj.gt.3300938.

[23] Guo P, El-Gohary Y, Prasadan K, Shiota C, Xiao X, Wiersch J, *et al*. Rapid and simplified purification of recombinant adeno-associated virus. Journal of Virological Methods. 2012; 183: 139–146. https://doi.org/10.1016/j.jviromet.2012.04.004.

[24] Starikova AV, Skopenkova VV, Polikarpova AV, Reshetov DA, Vassilieva SG, Velyaev OA, *et al*. Therapeutic potential of highly functional codon-optimized microutrophin for muscle-

specific expression. Scientific Reports. 2022; 12: 848. https://doi.org/10.1038/s41598-022-04892-x.
[25] Cazalets JR, Borde M, Clarac F. Localization and organization of the central pattern generator for hindlimb locomotion in newborn rat. The Journal of Neuroscience. 1995; 15: 4943–4951. https://doi.org/10.1523/JNEUROSCI.15-07-04943.1995.
[26] Nishimaru H, Restrepo CE, Ryge J, Yanagawa Y, Kiehn O. Mammalian motor neurons corelease glutamate and acetylcholine at central synapses. Proceedings of the National Academy of Sciences of the United States of America. 2005; 102: 5245–5249. https://doi.org/10.1073/pnas.0501331102.
[27] Steuer I, Guertin PA. Central pattern generators in the brainstem and spinal cord: an overview of basic principles, similarities and differences. Reviews in the Neurosciences. 2019; 30: 107–164. https://doi.org/10.1515/revneuro-2017-0102.
[28] Pikov V, Bullara L, McCreery DB. Intraspinal stimulation for bladder voiding in cats before and after chronic spinal cord injury. Journal of Neural Engineering. 2007; 4: 356–368. https://doi.org/10.1088/1741-2560/4/4/002.
[29] Watson C, Paxinos G, Kayalioglu G, Heise C. Atlas of the Rat Spinal Cord. In Watson C, Paxinos G, Kayalioglu G (eds.) The Spinal Cord (pp. 238–306). Academic Press: San Diego. 2009. https://doi.org/10.1016/B978-0-12-374247-6.50019-5.
[30] Toossi A, Bergin B, Marefatallah M, Parhizi B, Tyreman N, Everaert DG, *et al*. Comparative neuroanatomy of the lumbosacral spinal cord of the rat, cat, pig, monkey, and human. Scientific Reports. 2021; 11: 1955. https://doi.org/10.1038/s41598-021-81371-9.
[31] Storek B, Reinhardt M, Wang C, Janssen WGM, Harder NM, Banck MS, *et al*. Sensory neuron targeting by self-complementary AAV8 via lumbar puncture for chronic pain. Proceedings of the National Academy of Sciences of the United States of America. 2008; 105: 1055–1060. https://doi.org/10.1073/pnas.0708003105.
[32] Federici T, Taub JS, Baum GR, Gray SJ, Grieger JC, Matthews KA, *et al*. Robust spinal motor neuron transduction following intrathecal delivery of AAV9 in pigs. Gene Therapy. 2012; 19: 852–859. https://doi.org/10.1038/gt.2011.130.
[33] Mendell JR, Al-Zaidy S, Shell R, Arnold WD, Rodino-Klapac LR, Prior TW, *et al*. Single-Dose Gene-Replacement Therapy for Spinal Muscular Atrophy. The New England Journal of Medicine. 2017; 377: 1713–1722. https://doi.org/10.1056/NEJMoa1706198.
[34] Arber S, Han B, Mendelsohn M, Smith M, Jessell TM, Sockanathan S. Requirement for the homeobox gene Hb9 in the consolidation of motor neuron identity. Neuron. 1999; 23: 659–674. https://doi.org/10.1016/s0896-6273(01)80026-x.
[35] Talpalar AE, Bouvier J, Borgius L, Fortin G, Pierani A, Kiehn O. Dual-mode operation of neuronal networks involved in left-right alternation. Nature. 2013; 500: 85–88. https://doi.org/10.1038/nature12286.
[36] Sweeney LB, Bikoff JB, Gabitto MI, Brenner-Morton S, Baek M, Yang JH, *et al*. Origin and segmental diversity of spinal inhibitory interneurons. Neuron. 2018; 97: 341–355. https://doi.org/10.1016/j.neuron.2017.12.029.
[37] Francius C, Harris A, Rucchin V, Hendricks TJ, Stam FJ, Barber M, *et al*. Identification of multiple subsets of ventral interneurons and differential distribution along the rostrocaudal axis of the developing spinal cord. PLoS ONE. 2013; 8: e70325. https://doi.org/10.1371/journal.pone.0070325.
[38] Fowler CJ, Griffiths D, de Groat WC. The neural control of micturition. Nature Reviews. Neuroscience. 2008; 9: 453–466. https://doi.org/10.1038/nrn2401.
[39] Nathanson JL, Yanagawa Y, Obata K, Callaway EM. Preferential labeling of inhibitory and excitatory cortical neurons by endogenous tropism of adeno-associated virus and lentivirus vectors. Neuroscience. 2009; 161: 441–450. https://doi.org/10.1016/j.neuroscience.2009.03.032.
[40] Dougherty KJ, Kiehn O. Firing and cellular properties of V2a interneurons in the rodent spinal cord. The Journal of Neuroscience. 2010; 30: 24–37. https://doi.org/10.1523/JNEUROSCI.4821-09.2010.
[41] Zhang J, Lanuza GM, Britz O, Wang Z, Siembab VC, Zhang Y, *et al*. V1 and v2b interneurons secure the alternating flexor-extensor motor activity mice require for limbed locomotion. Neuron. 2014; 82: 138–150. https://doi.org/10.1016/j.neuron.2014.02.013.
[42] Goulding M. Circuits controlling vertebrate locomotion: moving in a new direction. Nature Reviews. Neuroscience. 2009; 10: 507–518. https://doi.org/10.1038/nrn2608.
[43] Berglund K, Clissold K, Li HE, Wen L, Park SY, Gleixner J, *et al*. Luminopsins integrate opto- and chemogenetics by using physical and biological light sources for opsin activation. Proceedings of the National Academy of Sciences of the United States of America. 2016; 113: E358–E367. https://doi.org/10.1073/pnas.1510899113.
[44] Gomez-Ramirez M, More AI, Friedman NG, Hochgeschwender U, Moore CI. The BioLuminescent-OptoGenetic in vivo response to coelenterazine is proportional, sensitive, and specific in neocortex. Journal of Neuroscience Research. 2020; 98: 471–480. https://doi.org/10.1002/jnr.24498.
[45] Yeh HW, Karmach O, Ji AH, Karmach J, Ji A, Carter D, *et al*. Red-shifted luciferase–luciferin pairs for enhanced bioluminescence imaging. Nat Methods. 2017; 14: 971–974. https://doi.org/10.1038/nmeth.4400.
[46] Rajput A, Pingale P, Dhapte-Pawar V. Nasal delivery of neurotherapeutics *via* nanocarriers: Facets, aspects, and prospects. Frontiers in Pharmacology. 2022; 13: 979682. https://doi.org/10.3389/fphar.2022.979682.
[47] Mizui Y, Eguchi M, Tanaka M, Ikeda Y, Yoshimura H, Ozawa T, *et al*. Long-term single cell bioluminescence imaging with C-3 position protected coelenterazine analogues. Organic & Biomolecular Chemistry. 2021; 19: 579–586. https://doi.org/10.1039/d0ob02020f.
[48] Zholudeva LV, Qiang L, Marchenko V, Dougherty KJ, Sakiyama-Elbert SE, Lane MA. The Neuroplastic and Therapeutic Potential of Spinal Interneurons in the Injured Spinal Cord. Trends in Neurosciences. 2018; 41: 625–639. https://doi.org/10.1016/j.tins.2018.06.004.
[49] Kuchimaru T. Emerging Synthetic Bioluminescent Reactions for Non-Invasive Imaging of Freely Moving Animals. International Journal of Molecular Sciences. 2024; 25: 7338. https://doi.org/10.3390/ijms25137338.
[50] Shen W, Liu S, Ou L. rAAV immunogenicity, toxicity, and durability in 255 clinical trials: A meta-analysis. Frontiers in Immunology. 2022; 13: 1001263. https://doi.org/10.3389/fimmu.2022.1001263.
[51] Ronzitti G, Gross DA, Mingozzi F. Human Immune Responses to Adeno-Associated Virus (AAV) Vectors. Frontiers in Immunology. 2020; 11: 670. https://doi.org/10.3389/fimmu.2020.00670.
[52] Ikefuama EC, Kendziorski GE, Anderson K, Shafau L, Prakash M, Hochgeschwender U, *et al*. Improved Locomotor Recovery in a Rat Model of Spinal Cord Injury by BioLuminescent-OptoGenetic (BL-OG) Stimulation with an Enhanced Luminopsin. International Journal of Molecular Sciences. 2022; 23: 12994. https://doi.org/10.3390/ijms232112994.